(Received 3 July 2026, Accepted 27 July 2026, Scheduled 27 July 2026)

Single-wavelength-driven DWDM Transmitter Chip on Monolithic Thin-film Lithium Niobate with a Record-high Spectral Efficiency

Shen Wang[1,†], Yuyi Wang[1,†], Haohua Wang[2,†], Yuntao Zhu[3,4], Junjie Yi[1], Defeng Shan[1], Mingwang Jiang[1], Jiakai Dong[3], Yunjie Wang[2], Jingyi Wang[4], Kaixuan Chen[2,5], Xinlun Cai[3], Jie Liu[3,*], Changjian Guo[2,5,*], Siyuan Yu[3], and Liu Liu[1,6,*]

[1]*State Key Laboratory of Extreme Photonics and Instrumentation*
Zhejiang Key Laboratory of Optoelectronic Information Technology
College of Optical Science and Engineering, East Bldg. No. 5, Zijingang Campus
Zhejiang University, Hangzhou 310058, China
[2]*Guangdong Provincial Key Laboratory of Optical Information Materials and Technology*
South China Academy of Advanced Optoelectronics, Sci. Bldg. No. 5
South China Normal University, Higher-Education Mega-Center, Guangzhou 510006, China
[3]*State Key Laboratory of Optoelectronic Materials and Technologies, School of Electronics and Information Technology*
Sun Yat-Sen University, Guangzhou 510006, China
[4]*Guangzhou Liobate Optoelectronics Limited, Guangzhou 510525, China*
[5]*National Center for International Research on Green Optoelectronics, South China Normal University, Guangzhou 510006, China*
[6]*Jiaxing Key Laboratory of Photonic Sensing & Intelligent Imaging, Intelligent Optics & Photonics Research Center*
Jiaxing Research Institute, Zhejiang University, Jiaxing 314000, China

ABSTRACT: Optical transmission based on dense wavelength-division multiplexing (DWDM) is widely considered a key solution for increasing optical-link capacity. However, the complexity and stringent requirements for optical devices in such systems challenge full integration on a chip. Here, we demonstrate the first monolithic DWDM transmitter chip, built on a thin-film lithium niobate. The chip consists of an easy-to-drive and high-efficiency electro-optical (EO) frequency comb generator for a flat-top multi-wavelength source, a single arrayed waveguide grating for both multiplexing and demultiplexing to ensure no wavelength misalignment, and an EO Mach-Zehnder modulator array. Using a single-wavelength laser as input, the proposed transmitter can deliver a total modulated signal of 1.6 Tbps in eight 100-GHz spacing channels using an intensity-modulation direct-detection scheme. A record high spectral efficiency of 2 bps/Hz was achieved for an integrated DWDM transmission system using optical frequency combs. The energy consumption of the entire system was measured to be 2.76 pJ/bit. This work establishes a scalable route towards a versatile and integrated multi-wavelength data processor for DWDM data transmissions, optical computing, and microwave-photonics.

1. INTRODUCTION

The growth of global data traffic, driven by cloud computing and artificial intelligence, has imposed unprecedented demands on optical interconnect infrastructures for short distances [1–3]. For data-centers and high-performance computing systems, the physical footprint and density of data interconnects, in addition to transmission capacities, increasingly become constraining factors for the scaling of these applications. Dense wavelength-division multiplexing (DWDM) is a technology that enables the simultaneous transmission of multiple independent data channels over a single physical channel, such as an optical fiber or waveguide. They have been proven to be efficient in improving the transmission density and throughput in long-haul optical communications [4–6]. However, for short-distance optical interconnects, the stringent requirements for optical devices make chip-scale DWDM system challenging to implement.

A core component of a DWDM transmitter is a multi-wavelength light source. Although traditional semiconductor lasers are technologically mature and reliable, packing them together in an array with a defined waveguide grid is still challenging. In this case, independent thermal stabilization and wavelength locking for each channel are required, which leads to a complex and bulky laser front-end [7]. Therefore, a single device that can deliver multiple wavelengths, that is, an optical frequency comb (OFC) device, is therefore more desirable. Semiconductor mode-locked laser (MLL)-based OFCs are the most energy-efficient and easier to package in a small form factor [8–10]. Using heterogeneous integration, it is also technically possible to build an integrated DWDM transceiver, together with modulators [11, 12]. However, owing to the complexity of fabrication, such a demonstration is lacking. Additionally, the most practical semiconductor MLLs still rely on InAs quantum dots, whose working wavelength

* Corresponding authors: Jie Liu (liujie47@mail.sysu.edu.cn), Changjian Guo (guochangjian@m.scnu.edu.cn), Liu Liu (liuliuopt@zju.edu.cn). † These authors contributed equally to this work.

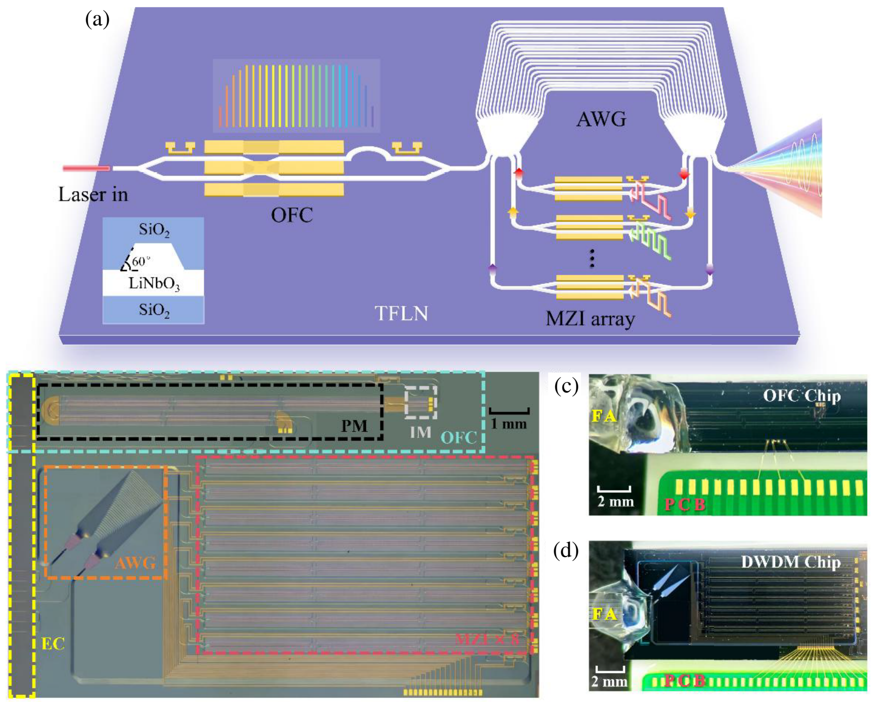

FIGURE 1. System schematic and fabricated chip of the present single-wavelength-driven eight-channel DWDM transmitter chip on monolithic TFLN. (a) Conceptual schematic of the transmitter. The input single-wavelength light is first expanded into a flat-top multi-wavelength source using the EO OFC generator, which is then demultiplexed into eight channels by an AWG. Data can be loaded on the light in each channel separately using integrated MZI modulators. The modulated optical signals from all channels are then multiplexed by the same AWG and finally output from the transmitter chip. The inset shows the cross-sectional sketch of the TFLN waveguide. (b) Optical microscope image of the final fabricated transmitter chip. The pitch between adjacent modulator channels is 625 μm. (c) & (d) Images of the packaged chips for the OFC generator and DWDM transmitter, respectively.

band is limited [8–10]. Based on nonlinear integrated micro-cavity resonators, Kerr OFCs can now generate hundreds of wavelengths coherently on a single chip with spectral spans covering one or more octaves [13–17]. By carefully tuning the material properties and/or resonant structures, the optical conversion efficiency of these optical nonlinearity based OFCs has reached ∼50% with a suitable wavelength span [18], and ultrahigh-bandwidth optical communications have also been demonstrated using these efficiency and span engineered Kerr OFCs as the light source [19, 20]. However, these procedures might pose some challenges in their further integration with multiplexers and modulators in a DWDM transmitter [17, 18]. The reconfigurability and control of the central wavelength and spectrum flatness of Kerr OFCs are also difficult [21, 22]. Electro-optical (EO) modulation-based OFCs offer, however, distinct advantages as compared to the above two technologies [23–25], including flat-top spectrum [26], continuously adjustable frequency spacing [27], and adjustable frequency span from several to over-900 comb lines [28]. The discrete form of this type of EO OFCs has also been successfully employed as a DWDM source in practical communication systems [29]. Additionally, it is straightforward to integrate EO OFCs with high-performance modulators on the same platform for multi-channel data transmissions.

Another core component of a DWDM transmitter is the wavelength (de)multiplexing device. The OFC sources need to be demultiplexed into individual wavelength channels, modulated with signals, and then multiplexed again for output. Naturally, the (de)multiplexing performances in terms of center wavelength alignment, insertion loss, and channel spacing uniformity is critical in the above process. Conventionally, cascaded micro-cavities, such as micro-rings [30–33] or Fabry-Perot cavities [34–36], are adopted for this purpose because they can act as (de)multiplexers and modulators simultaneously on a bus waveguide. This facilitates the achievement of a compact solution for DWDM transmitters. However, micro-cavity-based multiplexers have several drawbacks. First, each micro-cavity must be equipped with a feedback mechanism to compensate for resonant wavelength fluctuations due to fabrication variation or environmental temperature change. Since the number of cavities scales linearly with the number of wavelength channels, this imposes a large burden on the optical and electrical circuits for the necessary tuning, monitoring, and control functions [37, 38]. Second, the Q-factor of the cavity resonance should be carefully designed if it were to be used as a modulator. Considering the (de)multiplexing crosstalk, a high Q-factor is preferred because it allows a denser wavelength grid. On the other hand, a high-Q-factor cavity would largely decrease its modulation bandwidth owing to the long photon life-time [39]. The overall spectral efficiency is compromised in this case. In contrast, the arrayed waveguide grating (AWG) stands out as one of the most mature and scalable (de)multiplexing solutions

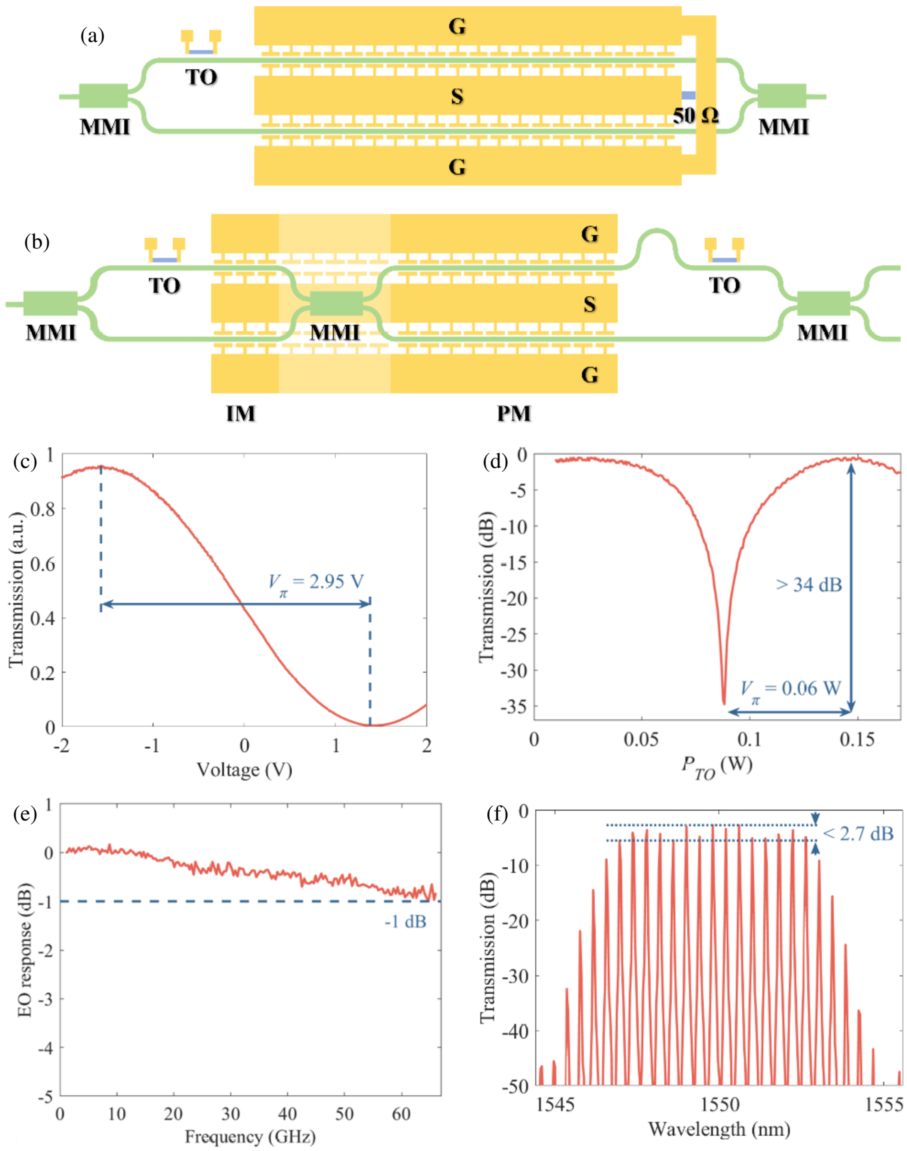

FIGURE 2. Structures and performances of the EO MZI modulator and OFC generator. (a) Sketch of the MZI modulator in the array consisting of a CLTW modulation section in a push-pull configuration terminated with an on-chip 50-Ω resistor, two MMIs, and a TO phase shifter section. (b) Sketch of the OFC generator consisting of an IM and a PM, which basically has the same electrode configuration as that in (a), except that the 50-Ω termination is designed off the chip, considering that a high microwave power should be used for the OFC generation. Normalized optical transmission of the MZI modulator (c) as a function of the applied modulation voltage driven by a 100-kHz sawtooth signal, and (d) as a function of the electrical power on the TO phase shifter. (e) Measured EO frequency response of the device. (f) Output spectrum of the OFC generator under a microwave drive of 50-GHz frequency and 35.5-dBm power.

on various platforms [40, 41], offering notable benefits, such as a high channel count up to 100 [42], a flat spectral response, and low channel crosstalk of −31.7 dB [43]. Crucially, owing to its fully symmetric configuration, a single AWG device inherently exhibits aligned center wavelengths across all channels when used concurrently as both multiplexer and demultiplexer, thereby substantially reducing the control complexity and footprint of the overall system.

In this study, we demonstrate, for the first time, a monolithically-integrated DWDM transmitter chip. As illustrated in Fig. 1(a), the present transmitter chip, built on the x-cut thin-film lithium niobate (TFLN) platform, mainly consists of three parts, that is, an EO OFC generator for an integrated multi-wavelength light source, an AWG (de)multiplexer, and an eight-channel modulator array for loading the data. In such an architecture, only a continuous-wave single-wavelength laser is required as the light source, and the output can then be expanded to modulated light in eight wavelength channels with 100-GHz channel spacing. The OFC generator is based on cascaded modulators, featuring only one microwave input and a measured on-chip optical conversion efficiency of 78.6% in a flat-top comb spectrum covering 800 GHz span. A single 9 × 9 AWG with 100-GHz channel spacing simultaneously functions as both a multiplexer

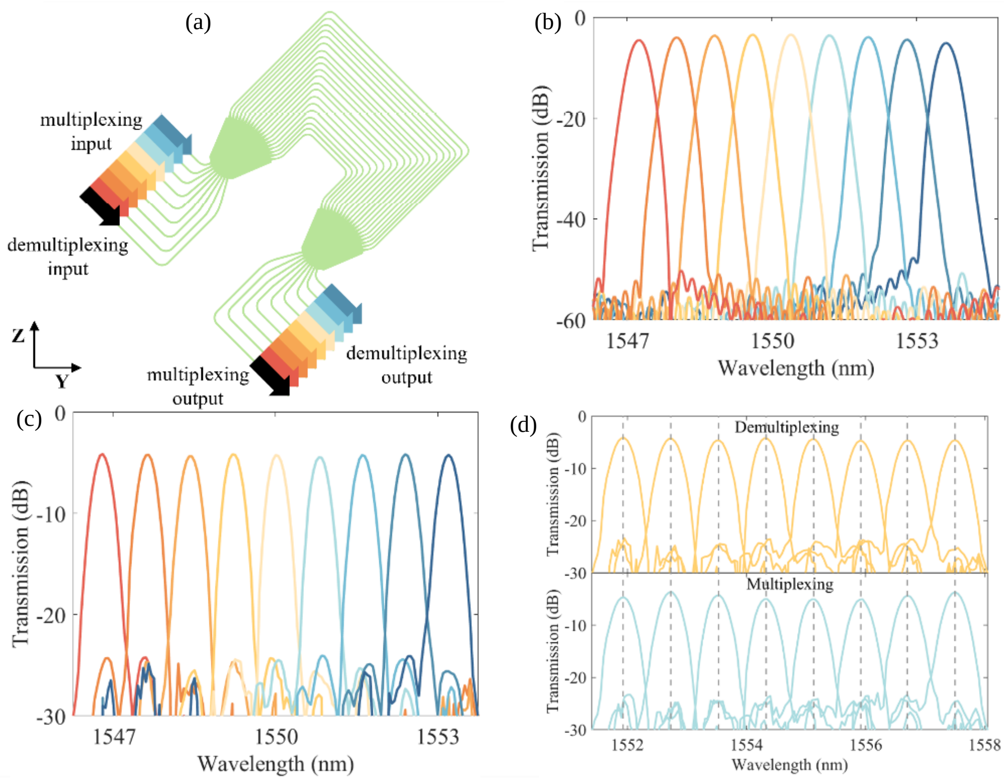

FIGURE 3. Structure and performances of the AWG (de)multiplexer. (a) Structure and working principle of the AWG in the present DWDM system. The multi-wavelength source from the OFC device is first input from one edge input port, and different wavelengths will be demultiplexed into different waveguides. After the modulators, the optical signal is routed back to the rest input ports of the AWG, and they will be multiplexed to one output waveguide in the same device. (b) Simulated and (c) measured output spectra of the AWG when inputting from the central port. (d) Measured output spectra of the AWG when used as a multiplexer and a demultiplexer for eight wavelengths in the present DWDM system, showing the strict wavelength alignment.

and demultiplexer. The fabricated AWG exhibited an insertion loss of 4.19 dB, adjacent-channel crosstalk of approximately −20 dB, and channel non-uniformities below 0.5 dB. The EO modulator in the array, adopting a Mach-Zehnder interferometer (MZI) structure, exhibits a nearly flat modulation response of up to 67 GHz. Successful data transmission of 200 Gbps on each channel was obtained, which led to an aggregated data rate of 1.6 Tbps. A record-high spectral efficiency of 2 bps/Hz and a transmission energy consumption of 2.76 pJ/bit was achieved using intensity-modulation direct-detection (IM-DD) scheme with this DWDM transmitter chip.

2. RESULTS

2.1. Transmitter Architecture

Several advanced designs were implemented in the DWDM transmitter chip shown in Fig. 1(a) to ensure highefficiency and wavelength robustness. The OFC generator consists of two modulators, where a phase modulator (PM) is employed to generate the comb lines, and an intensity modulator (IM) is used to shape the lines into a flat-top spectrum. Although this is a rather conventional scheme, we take advantage of the design flexibility for both optical and electrical structures on TFLN, and build such an OFC device with one common microwave input for both modulators and an on-chip coherent combining structure. These improvements help relieve the drive complexity and break the 50% constraint for optical conversion efficiency in this scheme. For the wavelength (de)multiplexer, a single multi-channel AWG is designed in an optical add-drop configuration, so that one such device can be used as a multiplexer and demultiplexer simultaneously. This helps eliminate any wavelength misalignment if separate devices are employed for these two functions. The AWG device is based on a 45° symmetry design on the x-cut TFLN platform [44, 45], which ensures seamless integration with the modulators. The modulator array consists of eight segmented MZI modulators, each equipped with a separate thermo-optic (TO) bias control electrode. As shown in Fig. 1(b), the components mentioned above, as well as other passive devices such as routing waveguides, multi-mode interference (MMI) power splitters, and bi-layer edge couplers (ECs) for fiber accesses, were all fabricated monolithically on a single x-cut lithium-niobate-on-insulator (LNOI) wafer. The TFLN waveguide structure has a thickness of 360 nm with an etched depth of 180 nm and an etched sidewall angle of 60°, and is embedded in silicon oxide. For the convenience of testing, the OFC generator part and the DWDM transmitter part (including the modulator array and AWG) of the chip were diced and packaged separately, as presented in Figs. 1(c) and 1(d).

2.2. EO Modulation Structure

The key part of the MZI modulator in each wavelength channel and the OFC generator shared the same EO modulation struc-

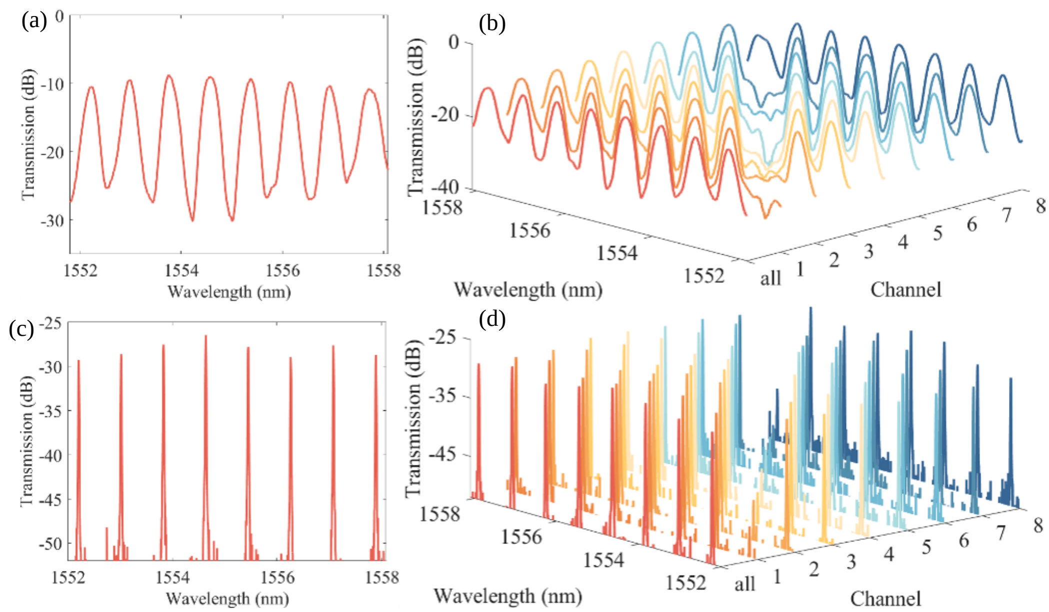

FIGURE 4. Static transmission and switching performance of the DWDM transmitter. Output spectra of (a) all channels turned on or (b) sequentially turned off by tuning the TO phase shifters in the modulator array, measured with a broadband light source. Output spectra of (c) all channels turned on or (d) sequentially turned off, when using the multi-wavelength source from the present OFC device as the input.

ture as depicted in Figs. 2(a) and 2(b). A periodic capacitively-loaded travelling-wave (CLTW) electrode is adopted to realize a high bandwidth, low optical loss, and high modulation efficiency [46]. Using the optimized parameters, a typical MZI modulator in the array with a modulation length of 8.02 mm in a push-pull configuration experimentally exhibits a half-wave voltage V_π of 2.95 V, which corresponds to a half-wave-voltage-length product $V_\pi L$ of 2.37 Vcm, an optical insertion loss of $\sim$0.5 dB, and a static extinction ratio of >34 dB as presented in Figs. 2(c) and 2(d). The measured small-signal EO frequency response of the device remained flat with a roll-off of only $\sim$1 dB at 67 GHz as shown in Fig. 2(e). The measured performances of all eight MZI modulators in the array are presented in Supplementary Note 1. The high performance of the modulation section facilitates high data-rate transmission in each wavelength channel, as well as high-efficiency flat-top OFC generation. Additionally, for low-speed bias tuning, a TO phase shifter was adopted on a TFLN waveguide. Using a heated waveguide length of 0.565 mm, a half-wave power P_π of 60 mW was measured as illustrated in Fig. 2(d). For the OFC device sketched in Fig. 2(b), the input light is first processed by an IM driven between its maximal and minimal transmissions, and the two light pulses from the complementary output arms of the IM are further modulated by a PM. The optical and microwave group delay between the two modulators were carefully tuned on the chip to fulfill the flat-top condition for the generated OFCs [27, 47]. After the PM and delay waveguide in one arm, the two outputs are combined coherently again. This leads to a flat-top OFC output with a theoretically 100% conversion efficiency for the optical signal. Practically, the critical parameters of the implemented OFC device, including the lengths of the PM and IM, the microwave driving voltage and frequency, are carefully designed to match the wavelength grid and span in the DWDM transmission. Fig. 2(f) shows the measured output spectrum from the fabricated OFC, which exhibits a wavelength spacing of 50 GHz, flat-top span of $\sim$800 GHz, and power non-uniformity of <2.7 dB. The measured on-chip optical conversion efficiency reached 78.6%, slightly less than 100%, which was mainly attributed to the optical insertion losses of the IM and PM. Every other wavelength line in this OFC is filtered and used as the light source for the following DWDM transmitter. The detailed working principle and design parameters of the OFC device are discussed in Supplementary Note 2.

2.3. AWG (De)multiplexer Structure

Considering the scalability and wavelength uniformity, an AWG was used to build the wavelength (de)multiplexer. To address the issue of propagation-direction related mode indices caused by the inherent uniaxial anisotropy of the x-cut TFLN, we adopted a 45° symmetry design for the AWG layout, where the symmetrical axis of the arrayed waveguides was aligned at 45° to the yz axes of the lithium niobate crystal. This strategy has been demonstrated to support good wavelength (de)multiplexing performances with channel spacings of down to 200 GHz. In this study, a 100-GHz channel-spacing AWG in the C-band was further optimized and fabricated to support DWDM transmissions. Additionally, nine input and output ports were designed for the AWG, so that it could be configured as an optical add-drop filter for eight wavelengths as shown in Fig. 3(a). The simulated and measured spectral responses of the AWG from all output ports are presented in Fig. 3(b) when input from the central port. The channel spacing is maintained accurately at 0.8 nm or 100 GHz. The measured responses when input from the central port are shown in Fig. 3(c) for a standalone AWG as a reference. Insertion losses of $\sim$4.2 dB, crosstalk from the adjacent channels of ~-20 dB, and channel non-uniformities of <0.4 dB can be extracted. Owing to fabrication variations, a slight deviation exists

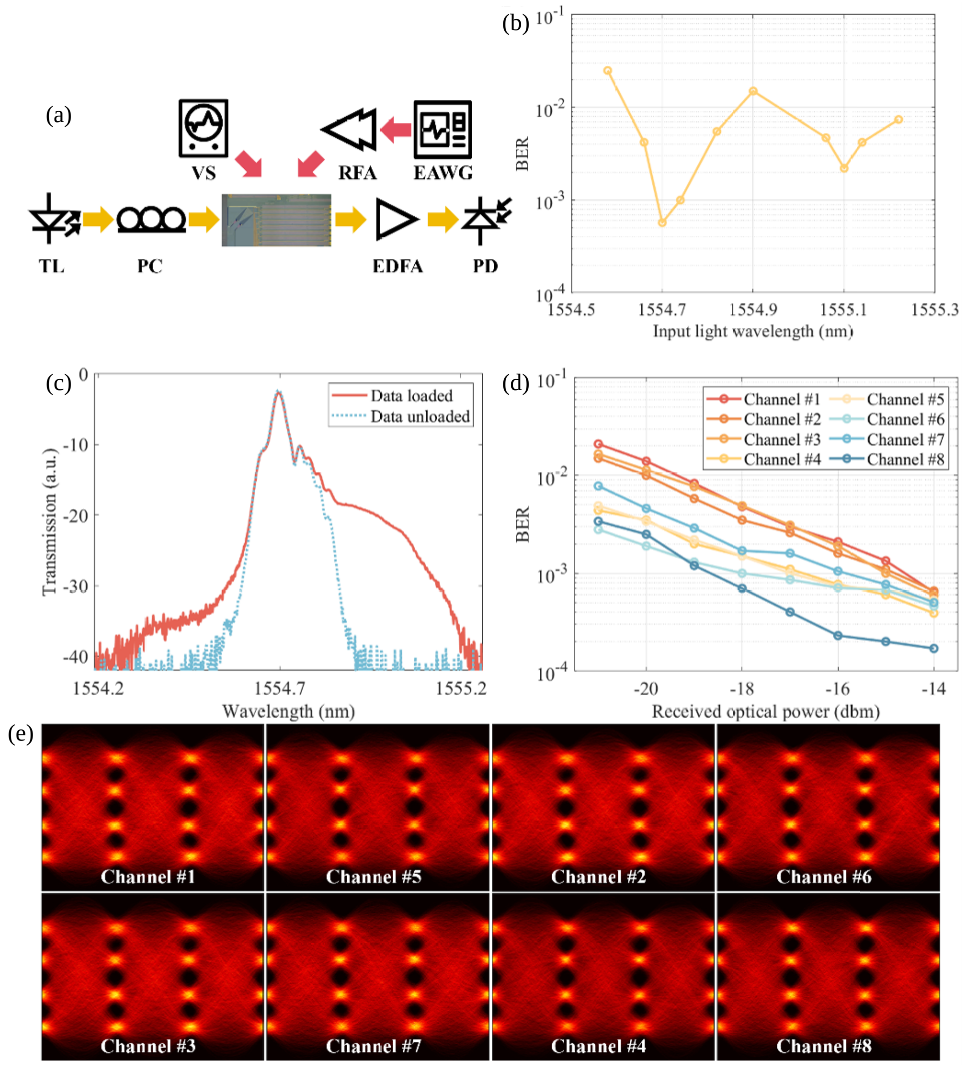

FIGURE 5. Performances of the DWDM transmitter under 100-GBaud PAM4 modulation when measured with an external tunable laser. (a) Experimental set-up for measuring the single-channel BERs. (b) BERs as a function of the input wavelength for channel #5. (c) Output spectra from channel #5 with data loaded or unloaded at 1554.7 nm. (d) BERs as a function of the received optical power for all eight channels. (e) Optical eye diagrams for all eight channels at received optical power of −14 dBm.

between the simulated and measured central wavelengths. Nevertheless, this discrepancy does not affect the subsequent system measurements because the fabrication-induced shift of the absolute AWG central wavelength is predominantly a common-mode offset, and can therefore be compensated by tuning the input laser wavelength of the OFC. Practically, the edge ports are used as inputs and outputs for demultiplexing and multiplexing, respectively. Notably, owing to the inherent symmetry of the device, the central wavelengths from all channels in multiplexing and demultiplexing are strictly aligned, as shown in Fig. 3(d). In traditional schemes, separate devices are used for multiplexing and demultiplexing processes. Even if the same device structure is adopted, the practical spectral responses may still show large variations owing to fabrication uncertainties. This would result in additional insertion losses and crosstalk in a DWDM transmission system [38]. This problem is completely avoided in the present configuration. The detailed design procedure, parameters, and fabrication variations of the AWG device are discussed in Supplementary Note 3.

2.4. DWDM IM-DD Transmission Performances

To evaluate the performance of the entire DWDM transmitter chip, a series of static switching experiments were designed and conducted. First, a broadband light source in the C-band was used to test the DWDM transmitter, as shown in Fig. 1(d). Initially, the voltages applied to the TO phase shifters of the modulators were adjusted to set all the channels to their maximal transmission points. The results, shown in Fig. 4(a), indicate on-chip insertion losses of ∼10 dB for each channel, which include the multiplexing and demultiplexing losses of ∼4.2 dB each and the modulator loss of ∼0.5 dB, as mentioned above. The coupling loss from chip to fiber is excluded here, which was measured to be ∼1.5 dB to a standard single-mode fiber across the whole C-band. Subsequently, each channel was turned off individually by tuning the TO phase shifters to their extinction points, while the output optical spectra were recorded. As shown in Fig. 4(b), turning off a single channel resulted in negligible variations in the other channels, with a maximal power fluctuation of less than 0.35 dB. These re-

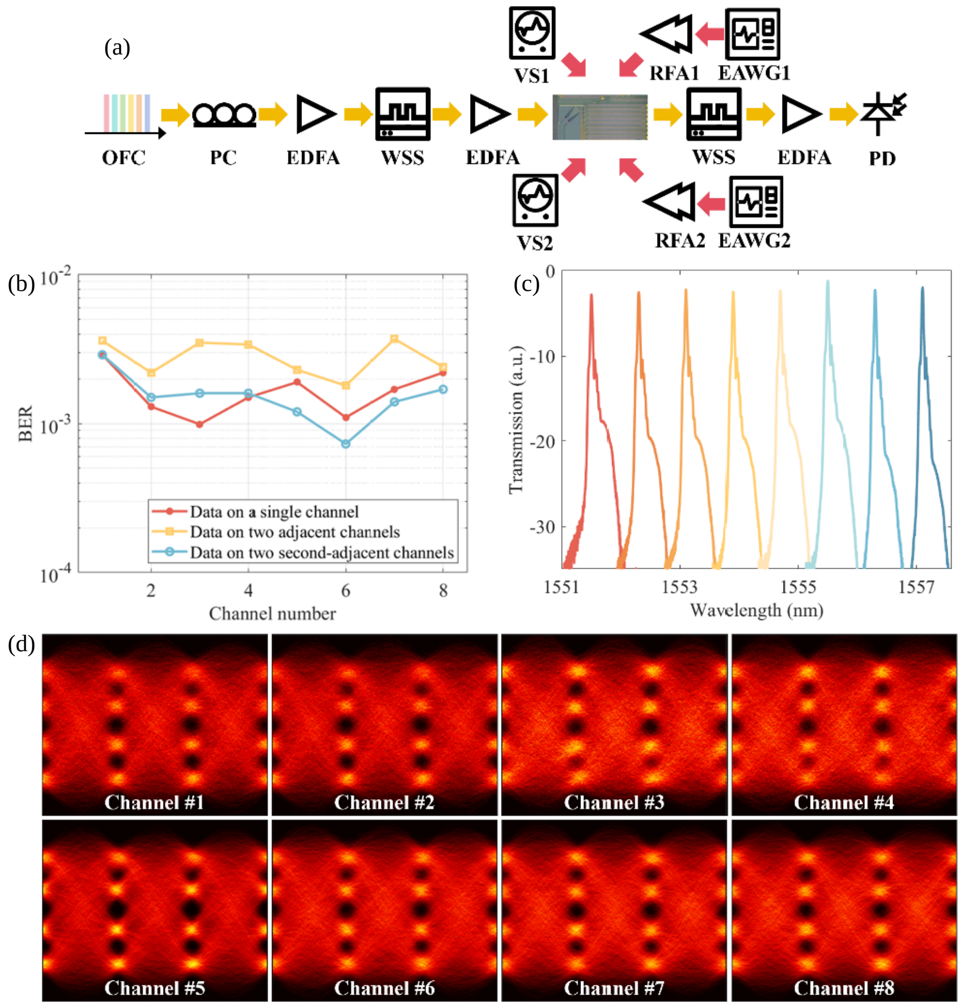

FIGURE 6. Performances of the complete DWDM transmitter under 100-GBaud PAM4 modulation using the EO OFC as the multi-wavelength source. (a) Experimental setup. (b) Measured BERs of the eight channels when data are applied to the target channel only, to the target channel and one adjacent channel, or to the target channel and one second-adjacent channel. (c) Overlaid output spectra of the eight wavelength channels with all optical carriers activated. (d) Measured eye diagrams at an ROP of −17 dBm when the target and one adjacent channel are simultaneously modulated.

sults indicate very low thermal and optical crosstalk in the proposed device. Next, the broadband source was replaced with the multi-wavelength source of the fabricated OFC device, as shown in Fig. 1(c). Again, all channels were turned on first and then off individually by adjusting the TO phase shifters. The output spectra are shown in Figs. 4(c) and 4(d). All channels exhibited extinction ratios of ∼20 dB. These results verify the excellent static switching performance of the proposed system. Further spectral details are available in Supplementary Note 4.

The DWDM part of the chip was first assessed for high-speed data transmission using the IM-DD setup shown in Fig. 5(a). Due to the relatively small channel spacing (100 GHz) and the resulting narrow 3 dB bandwidth (approximately 0.4 nm) of the AWG, a strong filtering effect would be expected for the modulated optical signal, which would limit the maximal baud rate per channel. Therefore, in order to fully exploit the available bandwidth and improve the spectral efficiency, a vestigial sideband (VSB) modulation scheme was adopted here, whereby the input optical wavelength was shifted relative to the central wavelength of each channel. Taking a 100-Gbaud PAM4 signal and channel #5 as an example, the original double-sideband signal cannot fit in the channel bandwidth of the present AWG, and a high bit error rate (BER) was measured as shown in Fig. 5(b). When the input wavelength was detuned from the center (1554.9 nm), the BER initially decreased and then increased again. The minimal BER was observed at an input wavelength of 1554.7 nm, where only the sideband at the longer wavelength of this 100-Gbaud PAM4 signal is filtered out, as also demonstrated in Fig. 5(c). The VSB modulation is theoretically studied in Supplementary Note 5 for all eight channels based on the measured spectrum responses of the AWG. The optimal detuning magnitudes fall within a relatively narrow range of approximately 0.21–0.26 nm, in good agreement with the experimentally measured value. Because the wavelength detuning cannot be optimized independently for each channel when an OFC source is used. A common blue detuning of approximately 0.2 nm was consequently selected for subsequent high speed data transmission testing, since it lies within the low-

TABLE 1. Characteristics of some integrated DWDM transmission systems using OFCs.

Ref.	Architecture	Capacity (Gbps)	Spectral efficiency (bps/Hz)	Energy consumption (fJ/bit)
[38]	InAs MLL OFC chip & Si micro-ring modulator array chip	8 × 100	1	1656 (total) 416 (modulator)
[11]	InAsMLL OFC chip & GaAs/Si micro-ring modulator array chip	8 × 25	0.42	2100 (total) 500 (modulator)
[17]	AlGaAs Kerr OFC chip, discrete (de)multiplexer, & Si MZI modulator array chip	20 × 100	0.56	-
[2]	SiN Kerr OFC chip & Si micro-disk modulator array chip	32 × 16	0.1	4900 (total) 1681.5 (modulator)
[37]	SiN Kerr OFC chip & Si micro-ring modulator array chip	20 × 128	1.28	5854 (total) 322.6 (modulator)
[29]	Discrete EO OFC & Si micro-ring modulator array chip	4 × 100	1.25	300 (modulator)
This work	Monolithically integrated TFLN chips with EO OFC, AWG, & MZI modulator array	8 × 200	2	2760 (total) 357.5 (modulator)

BER operating region of all eight channels. The BERs under varying received optical power levels were tested for all eight channels individually. The results are shown in Fig. 5(d). At a received optical power of -17 dBm, all channels achieved an BER below 3.8×10^{-3}, that is, the hard-decision forward error correction (HD-FEC) limit. At a received optical power of -14 dBm, all channels achieved BERs below 6.6×10^{-4}. The corresponding eye diagrams for the eight channels are shown in Fig. 5(e). All eye diagrams exhibit wide eye openings, clear and sharp crossing points, and symmetry, indicating excellent signal quality.

The performance of the full DWDM transmitter, utilizing the OFC device to generate the multi-wavelength source, was tested using the setup shown in Fig. 6(a). The desired output comb lines from the OFC were filtered out using a commercial wavelength-selective switch (WSS) before being sent to the DWDM part for subsequent measurements. The VSB procedure mentioned above was also implemented here, which can be realized simultaneously for all channels by tuning the wavelength of the input light to the OFC device. This would shift the entire comb spectrum collectively to the AWG for all channels, since the frequency spacing between the comb lines remains fixed. First, the single-channel BERs were measured by applying the 100 GBaud PAM4 signal to only one channel at a time. The BERs at a received optical power of -17 dBm are shown by the red line in Fig. 6(b), which are similar to those achieved with the tunable laser source at the same received power as discussed above. The power budget for the present communication system is discussed in Supplementary Note 6. Fig. 6(c) shows the output spectra of all eight optical carriers activated, demonstrating the occupation of the complete 800-GHz spectral span. Next, the crosstalk performance of the proposed transmitter was investigated. The pure EO crosstalk between different channels was measured first and is discussed in Supplementary Note 7. To study the influence of the EO crosstalk, as well as the optical crosstalk, on the data transmission performance. Two tests were conducted with two channels activated simultaneously. In the first scenario, modulation signals were applied to two adjacent channels, whereas the output from one channel was filtered out before the receiver for characterizations. The results, shown by the yellow line in Fig. 6(b), indicate slightly higher BERs, as compared to the case where only one channel is on in the same figure, but still below the HD-FEC limit. The corresponding eye diagrams for all eight channels are presented in Fig. 6(d). In the second scenario, the crosstalk from the second adjacent channel was tested. The results, depicted by the cyan line in Fig. 6(b), show BERs comparable to the single-channel cases, indicating negligible crosstalk from the second adjacent channel or channels further away in the proposed system. Due to the limited resources of high-speed EAWGs, only two channels can be activated simultaneously. To further assess the transmitter performance when all channels are loaded with data, we further performed measured-response-based numerical simulations using the experimentally obtained AWG multiplexing and demultiplexing spectra as presented in Supplementary Note 7. The results suggest that the dominant optical crosstalk indeed originates from the immediately adjacent AWG channel. Once one adjacent channel is activated, additional data loading from the other channels introduces only a minor further degradation. It can then be concluded that a good data transmission capability can be achieved with the present chip when all channels are activated.

3. CONCLUSION

In summary, this study demonstrated a monolithic IM-DDDWDM transmitter chip, which was realized on a TFLN platform and required only a single-wavelength laser input.

A total transmission capacity of 1.6 Tbps (8×200 Gbps) in a spectral span of 800 GHz (8×100 GHz) was achieved in the present transmitter. The EO OFC device using only one microwave electrode exhibited a high on-chip optical conversion efficiency of 78.6% with a flat-top spectrum. A single multi-channel AWG with symmetric input and output wavelength responses was designed to perform both multiplexing and demultiplexing functions. These designs not only significantly reduce the chip footprint but also reduce the complexity of wavelength alignment between the OFC device, multiplexer, and demultiplexer structures, which is a common challenge in other schemes. Table 1 summarizes the characteristics of recent demonstrations of DWDM transmission systems utilizing OFCs. Clearly, this study highlights the highest spectral efficiency of 2 bps/Hz for an integrated transmission system using OFCs. The total energy consumption of the transmitter system was estimated to be 2.76 pJ/bit with the main portion used for generating the OFC. This figure is already smaller than those using Kerr OFCs as the multi-wavelength source, but is still higher than those using MLLs. Nevertheless, by optimizing the OFC generator structure, the total energy consumption is anticipated to decrease to $\sim$500 fJ/bit. A detail discussion on energy consumption is presented in Supplementary Note 8.

In the present chip, the OFC frequency spacing is half of the AWG channel spacing, leading to an inefficient utilization of comb power. This can be solved by redesigning the OFC or AWG devices to match their channel spacings. Another strategy is to include a wavelength interleaver between the present OFC and AWG devices, as discussed in Supplementary Note 9, to form a space division multiplexing scheme [48]. In this case, a 3.2-Tbps DWDM transmitter can be readily obtained. It can also help improve the power budget of the whole system as discussed in Supplementary Note 6. The TO tuning employed for the OFC and MZI devices can be replaced by the bias-embedded modulation electrode design [49], which enables a capacitive EO bias tuning without introducing any additional optical structures. This facilitates a decrease in the device footprint and energy consumption. The proposed DWDM transmitter structure can also be easily scaled to a higher channel count by optimizing the microwave power to the OFC device, as well as the lengths of the IM and PM, for generating more comb lines, and increasing the number of input/output waveguides of the AWG. A coherent DWDM transmitter is also feasible by simply replacing the MZI intensity modulators with IQ modulators. This can further improve the aggregate data rate, receiver sensitivity, and spectral efficiency. Looking forward, this work establishes a scalable route towards versatile and integrated multi-wavelength data processing on the monolithic TFLN platform for not only DWDM data transmissions, but also possible applications in, for example, optical convolution streaming processors [50] and channelized microwave-photonic transmitters and receivers [51].

EXPERIMENTAL SECTION

Chip fabrication and packaging were performed. The present DWDM transmitter chip was fabricated using a commercial TFLN PDK (Liobate Technology Co., Ltd., China). A 6-inch LNOI wafer (Shanghai Novel Si Integration Technology Co., Ltd., China) of 360-nm top TFLN layer on a buried silicon oxide layer and a silicon substrate was adopted. Two layers of TFLN patterns were first fabricated using 248-nm deep-ultraviolet (DUV) lithography and dry etching. A silicon oxide over-cladding layer of $\sim$1-μm thickness was subsequently deposited using plasma enhanced chemical vapor deposition. Metal patterns including microwave modulation electrodes made of Au, TO heaters, and termination resistors made of Ni/Cr, were defined using DUV lithography, thermal evaporation, and lift-off technologies. After the wafer fabrication, the chips were diced, and the coupling facets were mechanically polished. The finished chips were mounted on printed circuit boards (PCBs), where the low-speed TO tuning electrodes were routed using wire bonding. Matched fiber arrays (FAs) were aligned and attached to the chip edge. The high-speed modulation electrodes and pads were left intact and accessed using microwave probes during the measurements.

High-speed data transmission measurements. For OFC generation, single-wavelength light from a tunable laser (TL) was coupled to the OFC chip using a fiber-based polarization controller (PC). A 50-GHz sinusoidal electrical signal from an analog microwave source was amplified and applied to the chip through a 67-GHz microwave probe with a ground-signal-ground (GSG) configuration (GGB 67A). Another GSG probe was used to connect an external 50-Ω termination to the OFC chip. The generated OFC was then amplified to $\sim$23 dBm by a high-power erbium-doped fiber amplifier (EDFA) and sent to a programmable WSS (WaveShaper, Finisar), which selected eight mutually coherent comb lines with 100-GHz spacing from the original 50-GHz-spaced OFC. For data modulation, either the filtered comb lines or a single-wavelength laser directly from the TL were coupled into the DWDM transmitter chip. Owing to the limitation of the available microwave probing configuration (GSGGSG dual probe), only two channels can be driven with data simultaneously. The 100-Gbaud PAM4 electrical signals were generated by an electrical arbitrary waveform generator (EAWG, Keysight M8199B, 128 GSa/s), amplified by a linear microwave amplifier (RFA, SHF 807C), and then applied to the modulators. The bias point of the modulator was controlled using a voltage source (VS). At the output, the channel under test was selected using another WSS, and the optical signal was detected with a pre-amplified receiver consisting of another EDFA and a 70-GHz photodetector (PD, Finisar XPDV 3120). The optical power arriving before the EDFA is considered the received optical power. The final electrical signal was captured using a real-time oscilloscope with a 59-GHz analog bandwidth and 160 GSa/s sampling rate (Lecroy LabMaster 10-59Zi-A). Offline digital signal processing, including resampling, timing phase recovery, and 21-tap feed-forward equalization plus 5-tap decision feedback equalization, was performed to evaluate the BERs and eye-diagrams.

ACKNOWLEDGEMENT

This work was partially supported by the National Natural Science Foundation of China (grant Nos. 62435016 and 62135012), Key Research and Development Program of Guangdong Province (grant No. 2025B0101180003), Basic and Applied Basic Research Foundation of Guangdong Province (grant No. 2024A1515011710), Guangdong Provincial Key Laboratory of Optical Information Materials and Technology (grant No. 2023B1212060065), and Science and Technology Planning Project of Guangdong Province (grant No. 2019A050510039).

REFERENCES

[1] Pfeifle, J., V. Brasch, M. Lauermann, Y. Yu, D. Wegner, T. Herr, K. Hartinger, P. Schindler, J. Li, D. Hillerkuss, *et al.*, "Coherent terabit communications with microresonator Kerr frequency combs," *Nature Photonics*, Vol. 8, No. 5, 375–380, 2014.

[2] Rizzo, A., A. Novick, V. Gopal, B. Y. Kim, X. Ji, S. Daudlin, Y. Okawachi, Q. Cheng, M. Lipson, A. L. Gaeta, and K. Bergman, "Massively scalable Kerr comb-driven silicon photonic link," *Nature Photonics*, Vol. 17, No. 9, 781–790, 2023.

[3] Winzer, P. J. and D. T. Neilson, "From scaling disparities to integrated parallelism: A decathlon for a decade," *Journal of Lightwave Technology*, Vol. 35, No. 5, 1099–1115, 2017.

[4] Ataie, V., E. Temprana, L. Liu, E. Myslivets, B. P.-P. Kuo, N. Alic, and S. Radic, "Ultrahigh count coherent WDM channels transmission using optical parametric comb-based frequency synthesizer," *Journal of Lightwave Technology*, Vol. 33, No. 3, 694–699, 2015.

[5] Corcoran, B., M. Tan, X. Xu, A. Boes, J. Wu, T. G. Nguyen, S. T. Chu, B. E. Little, R. Morandotti, A. Mitchell, and D. J. Moss, "Ultra-dense optical data transmission over standard fibre with a single chip source," *Nature Communications*, Vol. 11, No. 1, 2568, 2020.

[6] Jørgensen, A. A., D. Kong, M. R. Henriksen, F. Klejs, Z. Ye, O. B. Helgason, H. E. Hansen, H. Hu, M. Yankov, S. Forchhammer, P. Andrekson, A. Larsson, M. Karlsson, J. Schröder, Y. Sasaki, K. Aikawa, J. W. Thomsen, T. Morioka, M. Galili, V. Torres-Company, and L. K. Oxenløwe, "Petabit-per-second data transmission using a chip-scale microcomb ring resonator source," *Nature Photonics*, Vol. 16, No. 11, 798–802, 2022.

[7] Grillanda, S., D. Che, M. H. Idjadi, C. Bolle, R. Kopf, and M. Cappuzzo, "Comb sources with hybrid photonic integration," in *2025 IEEE Photonics Conference (IPC)*, 1–2, Singapore, 2025.

[8] Dong, B., M. Dumont, O. Terra, H. Wang, A. Netherton, and J. E. Bowers, "Broadband quantum-dot frequency-modulated comb laser," *Light: Science & Applications*, Vol. 12, No. 1, 182, 2023.

[9] Hugi, A., G. Villares, S. Blaser, H. C. Liu, and J. Faist, "Mid-infrared frequency comb based on a quantum cascade laser," *Nature*, Vol. 492, No. 7428, 229–233, 2012.

[10] Rafailov, E. U., M. A. Cataluna, and W. Sibbett, "Mode-locked quantum-dot lasers," *Nature Photonics*, Vol. 1, No. 7, 395–401, 2007.

[11] Liang, D., S. Srinivasan, G. Kurczveil, B. Tossoun, S. Cheung, Y. Yuan, A. Descos, Y. Hu, Z. Huang, P. Sun, *et al.*, "An energy-efficient and bandwidth-scalable DWDM heterogeneous silicon photonics integration platform," *IEEE Journal of Selected Topics in Quantum Electronics*, Vol. 28, 1–19, 2022.

[12] Tossoun, B., X. Xiao, S. Cheung, Y. Yuan, Y. Peng, S. Srinivasan, G. Giamougiannis, Z. Huang, P. Singaraju, Y. London, *et al.*, "Large-scale integrated photonic device platform for energy-efficient AI/ML accelerators," *IEEE Journal of Selected Topics in Quantum Electronics*, Vol. 31, 1–26, 2025.

[13] Del'Haye, P., A. Schliesser, O. Arcizet, T. Wilken, R. Holzwarth, and T. J. Kippenberg, "Optical frequency comb generation from a monolithic microresonator," *Nature*, Vol. 450, 1214–1217, 2007.

[14] Gaeta, A. L., M. Lipson, and T. J. Kippenberg, "Photonic-chip-based frequency combs," *Nature Photonics*, Vol. 13, No. 3, 158–169, 2019.

[15] Kippenberg, T. J., A. L. Gaeta, M. Lipson, and M. L. Gorodetsky, "Dissipative Kerr solitons in optical microresonators," *Science*, Vol. 361, No. 6402, 129–162, 2018.

[16] Pasquazi, A., M. Peccianti, L. Razzari, D. Moss, S. Coen, M. Erkintalo, Y. K. Chembo, T. Hansson, S. Wabnitz, P. Del'Haye, *et al.*, "Micro-combs: A novel generation of optical sources," *Physics Reports*, Vol. 729, 1–81, 2018.

[17] Shu, H., L. Chang, Y. Tao, B. Shen, W. Xie, M. Jin, A. Netherton, Z. Tao, X. Zhang, R. Chen, *et al.*, "Bridging microcombs and silicon photonic engines for optoelectronics systems," *Nature*, Vol. 605, 457–463, 2022.

[18] Pirmoradi, A., J. Zang, K. Omirzakhov, Z. Yu, Y. Jin, S. B. Papp, and F. Aflatouni, "Integrated multi-port multi-wavelength coherent optical source for beyond Tb/s optical links," *Nature Communications*, Vol. 16, No. 1, 6387, 2025.

[19] Marin-Palomo, P., J. N. Kemal, M. Karpov, A. Kordts, J. Pfeifle, M. H. P. Pfeiffer, P. Trocha, S. Wolf, V. Brasch, M. H. Anderson, *et al.*, "Microresonator-based solitons for massively parallel coherent optical communications," *Nature*, Vol. 546, No. 7657, 274–279, 2017.

[20] Corcoran, B., A. Mitchell, R. Morandotti, L. K. Oxenløwe, and D. J. Moss, "Optical microcombs for ultrahigh-bandwidth communications," *Nature Photonics*, Vol. 19, No. 5, 451–462, 2025.

[21] Del'Haye, P., T. Herr, E. Gavartin, M. L. Gorodetsky, R. Holzwarth, and T. J. Kippenberg, "Octave spanning tunable frequency comb from a microresonator," *Physical Review Letters*, Vol. 107, No. 6, 063901, 2011.

[22] Papp, S. B., P. Del'Haye, and S. A. Diddams, "Mechanical control of a microrod-resonator optical frequency comb," *Physical Review X*, Vol. 3, No. 3, 031003, 2013.

[23] Chang, L., S. Liu, and J. E. Bowers, "Integrated optical frequency comb technologies," *Nature Photonics*, Vol. 16, No. 2, 95–108, 2022.

[24] Parriaux, A., K. Hammani, and G. Millot, "Electro-optic frequency combs," *Advances in Optics and Photonics*, Vol. 12, No. 1, 223–287, 2020.

[25] Zhuang, R., K. Ni, G. Wu, T. Hao, L. Lu, Y. Li, and Q. Zhou, "Electro-optic frequency combs: Theory, characteristics, and applications," *Laser & Photonics Reviews*, Vol. 17, No. 6, 2200353, 2023.

[26] Demirtzioglou, I., C. Lacava, K. R. H. Bottrill, D. J. Thomson, G. T. Reed, D. J. Richardson, and P. Petropoulos, "Frequency comb generation in a silicon ring resonator modulator," *Optics Express*, Vol. 26, No. 2, 790–796, 2018.

[27] Chen, G., Z. Ruan, and L. Liu, "High-efficiency and flat-top electro-optic frequency comb using a single modulator and drive on thin-film lithium niobate," *ACS Photonics*, Vol. 12, No. 2, 768–775, 2025.

[28] Zhang, M., B. Buscaino, C. Wang, A. Shams-Ansari, C. Reimer, R. Zhu, J. M. Kahn, and M. Lončar, "Broadband electro-optic frequency comb generation in a lithium niobate microring resonator," *Nature*, Vol. 568, No. 7752, 373–377, 2019.

[29] Kong, D., H. Xin, K. Kim, Y. Liu, L. K. Oxenløwe, P. Dong, and H. Hu, "Intra-datacenter interconnects with a serialized silicon optical frequency comb modulator," *Journal of Lightwave Technology*, Vol. 38, No. 17, 4677–4682, 2020.

[30] Yuan, Y., Y. Peng, W. V. Sorin, S. Cheung, Z. Huang, D. Liang, M. Fiorentino, and R. G. Beausoleil, "A 5×200 Gbps microring modulator silicon chip empowered by two-segment Z-shape junctions," *Nature Communications*, Vol. 15, No. 1, 918, 2024.

[31] Chen, P., S. Chen, X. Guan, Y. Shi, and D. Dai, "High-order microring resonators with bent couplers for a box-like filter response," *Optics Letters*, Vol. 39, No. 21, 6304–6307, 2014.

[32] Guan, H., Z.-Y. Li, H.-H. Shen, and Y.-D. Yu, "Compact optical add-drop de-multiplexers with cascaded micro-ring resonators on SOI," *Chinese Physics Letters*, Vol. 34, No. 6, 064201, 2017.

[33] Xia, F., M. Rooks, L. Sekaric, and Y. Vlasov, "Ultra-compact high order ring resonator filters using submicron silicon photonic wires for on-chip optical interconnects," *Optics Express*, Vol. 15, No. 19, 11 934–11 941, 2007.

[34] He, J., M. Zhang, D. Liu, Y. Bao, C. Li, B. Pan, Y. Huang, Z. Yu, L. Liu, Y. Shi, and D. Dai, "Twelve-channel LAN wavelength-division multiplexer on lithium niobate," *Nanophotonics*, Vol. 13, No. 1, 85–93, 2024.

[35] Liu, H., B. Pan, H. Li, Z. Yu, L. Liu, Y. Shi, and D. Dai, "First demonstration of lithium niobate photonic chip for dense wavelength-division multiplexing transmitters," *Advanced Photonics*, Vol. 6, No. 6, 066001, 2024.

[36] Zhu, M., D. Liu, W. Wang, H. Zhong, F. Huang, S. Zhao, A. Gao, J. Gan, W. Zhao, C. Gao, *et al.*, "An 8×240 Gbps dense wavelength division multiplexing transmitter with lithium tantalate," *Nature Communications*, Vol. 16, 11365, 2025.

[37] Cai, H., Z. Liao, Y. Zhang, X. Zhang, C. Zhang, and Y. Yu, "Microcomb and micro-ring modulator driven DWDM optical transmitter with ultra-high speed of 20×128 Gb/s," *Journal of Lightwave Technology*, Vol. 43, No. 15, 7239–7245, 2025.

[38] Chen, J., B. Yang, J. Qin, J. Huang, X. Cui, J. Yan, D. Wu, X. Xiao, Z. Wang, C. Yu, *et al.*, "Energy efficient and high bandwidth quantum dot comb laser based silicon microring transmitter for optical interconnects," *IEEE Journal of Selected Topics in Quantum Electronics*, Vol. 31, No. 2, 1–10, 2025.

[39] Hu, F., F. Yu, X. Liu, A. Wang, X. Hu, H. Cai, and W. Chu, "400-Gbps/λ ultrafast silicon microring modulator for scalable optical compute interconnects," *Laser & Photonics Reviews*, Vol. 20, No. 13, e02840, 2026.

[40] Hulyal, S. U., D. Fang, J. Cai, A. Kotz, X. Ou, C. Koos, and T. J. Kippenberg, "A 1.6 Tbit/s WDM integrated photonic IMDD transmitter on thin-film lithium tantalate," in *Optical Fiber Communications Conference and Exhibition (OFC), 2026*, paper W1A.7, Technical Digest Series (Optica Publishing Group, 2026), 2026.

[41] Huang, F., X. Shen, S. Wang, H. Xu, H. Liu, Z. Wang, H. Gao, X. Yao, H. Cao, B. Chen, *et al.*, "Toward large-scale photonic chips using low-anisotropy thin-film lithium-tantalate," *Advanced Science*, Vol. 12, No. 9, 2410345, 2025.

[42] Tu, H., Y. Zhang, G. Li, X. Dai, Y. Wu, Y. Zhang, H. Li, Q. Lu, M. Lu, and W. Guo, "100-Channel arrayed waveguide grating based on thin film lithium niobate on insulator (LNOI)," *Journal of Lightwave Technology*, Vol. 42, No. 13, 4519–4524, 2024.

[43] Shen, X., C. Li, W. Zhao, H. Li, Y. Shi, and D. Dai, "Ultra-low-crosstalk silicon arrayed-waveguide grating (de)multiplexer with 1.6-nm channel spacing," *Laser & Photonics Reviews*, Vol. 18, No. 1, 2300617, 2024.

[44] Pan, X., J. Yi, S. Wang, Z. Ruan, F. Huang, Z. Yu, D. Dai, and L. Liu, "Electrically and arbitrarily reconfigurable arrayed waveguide grating on thin film lithium niobate," *Laser & Photonics Reviews*, Vol. 19, No. 20, e00507, 2025.

[45] Yi, J., C. Guo, Z. Ruan, G. Chen, H. Wei, L. Lu, S. Gong, X. Pan, X. Shen, X. Guan, D. Dai, K. Zhong, and L. Liu, "Anisotropy-free arrayed waveguide gratings on X-cut thin film lithium niobate platform of in-plane anisotropy," *Light: Science & Applications*, Vol. 13, No. 1, 147, 2024.

[46] Chen, G., K. Chen, R. Gan, Z. Ruan, Z. Wang, P. Huang, C. Lu, A. P. T. Lau, D. Dai, C. Guo, and L. Liu, "High performance thin-film lithium niobate modulator on a silicon substrate using periodic capacitively loaded traveling-wave electrode," *APL Photonics*, Vol. 7, No. 2, 026103, 2022.

[47] Cheng, R., X. Ren, C. Reimer, M. Yeh, V. Rosborough, J. Musolf, L. Johansson, M. Zhang, M. Yu, and M. Lončar, "Single-drive electro-optic frequency comb source on a photonic-wire-bonded thin-film lithium niobate platform," *Optics Letters*, Vol. 49, No. 12, 3504–3507, 2024.

[48] Li, S., P. Yuan, T. Li, B. Li, R. Xu, Y. Yang, and L. Zhu, "High-performance interrogator with bilateral input MMI-based AWG," *Optics Letters*, Vol. 49, No. 3, 454–457, 2024.

[49] Jiang, M., G. Chen, R. Gan, H. Wang, D. Shan, Z. Ruan, B. Chen, L. Qi, X. Wu, W. Yang, *et al.*, "Thin-film lithium niobate traveling-wave modulators with embedded DC-bias electrode," *Laser & Photonics Reviews*, Vol. 20, No. 4, e02031, 2026.

[50] Wang, J., X. Xu, X. Zhu, Y. Xu, S. Chen, H. Zhang, Y. Zheng, S. Li, Y. Bai, Z. Liu, *et al.*, "Microcomb-enabled parallel self-calibration optical convolution streaming processor," *Light: Science & Applications*, Vol. 15, No. 1, 149, 2026.

[51] Song, X., X. Zhang, X. Gao, Z. Wang, J. Cai, Z. Tu, J. Dong, S. Li, Z. Zhou, J. Huang, *et al.*, "Full dimensional control of structured microwaves based on microcombs," *Nature Photonics*, Vol. 20, No. 4, 377–385, 2026.